DATASET BRIEF

Comparative proteomic study of early hypoxic response in the cerebral cortex of rats submitted to two different hypoxic models

David Ovelleiro[1], Santos Blanco[2]*, Raquel Hernández[2] and María Ángeles Peinado[2]*

[1] Area of Bioinformatics, Instituto Maimónides de Investigación Biomédica de Córdoba, Jaén, Spain
[2] Area of Cellular Biology, Department of Experimental Biology, University of Jaén, Jaén, Spain

Received: April 7, 2017
Revised: June 21, 2017
Accepted: June 30, 2017

Purpose: The present study analyses and compares the cortical brain proteomic profiles of two different models of cerebral hypoxic insult in rats (HH: hypobaric hypoxia and HHI: ischemia followed by hypobaric hypoxia) in an attempt to describe the alterations of the early molecular hypoxic adaptive response underlying each one.
Experimental Design: A quantitative proteomic profile of left-brain cortices of rats under HH, HHI, and control conditions was determined using isobaric labeling (Tandem Mass Tag™) on the protein extracts from pools of five individuals. Data are available via ProteomeXchange with identifier PXD004091.
Results: Altogether, 339 proteins were confidently quantified, 99 of them showing significant variations in the hypoxic conditions with respect to the control. The HHI model presents a global effect of protein downregulation while HH produces an overall increase of the protein levels. While HH mainly affecting oxidative and energetic metabolism, HHI also interferes with synaptic transmission, neurotransmitter secretion, *substantia nigra* development, and triggers apoptosis through mitochondrial pathway.
Conclusions and Clinical Relevance: The findings obtained show an overview of protein alterations under two hypoxic models of different aetiology and provide a basis for more detailed studies in order to unravel new specific mechanisms and therapies for hypoxic pathologies.

Keywords:
Hypoxia / Ischemia / Proteomics / TMT

Additional supporting information may be found in the online version of this article at the publisher's web-site

1 Introduction

Decline or complete deprivation of oxygen flow to brain and posterior reoxygenation represent a global health issue, as occur after an episode of hypobaric hypoxia or in the cerebral ischemic diseases [1]. Given that decrease or lack of oxygen characterizes all these illnesses, they share several molecular hallmarks: oxidative and nitrosative stresses [2], excitotoxicity [3] or apoptotic and necrotic neuronal death [4]. Nevertheless, the available data point out to specific patterns of these molecular responses depending on the multifactorial aetiology, duration, and severity of the hypoxic insult [5]. Certainly, these variables define and modulate the type of hypoxic adaptive response as well as the hypoxic damage, although the specific molecular pattern underlying each ones is still scarcely known. In the present work, we propose a quantitative analysis and comparison using isobaric labeling (TMT, Tandem Mass Tag™) of the proteomic profiles of two cerebral hypoxic models of different aetiology and scope, both simulating brain hypoxic pathologies: high altitude and cerebral ischemic disease.

Our study has been performed on 15 adult male Wistar rats provided by Harlan Laboratories (Envigo) and weighing

Correspondence: María Ángeles Peinado, Department of Experimental Biology, University of Jaén, Campus Las Lagunillas s/n, 23071 Jaén, Spain
E-mail: apeinado@ujaen.es

Abbreviations: **g.s.d**, global standard deviation; **GO**, Gene Ontology; **HH**, Hypobaric hypoxia; **HHI**, Ischemia followed by hypobaric hypoxia; **TMT**, Tandem Mass Tag™

*These authors have contributed equally to this work.

Colour Online: See the article online to view Figs. 1 and 2 in colour.

350 g each, kept under standard conditions of light and temperature and allowed ad libitum access to food and water, all procedures performed in accordance with the EU animal welfare directive 2010/63/EU. Animals were distributed into three different groups ($n = 5$ per group) depending on the hypoxic model: hypobaric hypoxia (HH), ischemia followed by hypobaric hypoxia (HHI) and a sham control group without any ischemic or hypoxic manipulations. The first one was submitted to a model of hypobaric hypoxia (HH) using a slight modification of a previously published procedure [6] by downregulating the environmental O_2 pressure to a final barometric pressure of approximately 300 hPa inside a hypobaric chamber. The rats were placed in the hypobaric chamber in which the air pressure was controlled by means of a continuous vacuum pump and an adjustable inflow valve. The conditions, simulating an altitude of 9144 m, were maintained for 1 h (temperature and humidity conditions being 23±1°C and 60–70%, respectively). Ascent and descent rates were kept below 300 m/min and the return to normobaric normoxic conditions spanned 30 min. The second group was submitted to a model of cerebral ischemia followed by hypobaric hypoxia (HHI), which consists of unilateral left common carotid artery occlusion followed by a hypoxic stress for a predetermined time, consisting of a slight modification of the Levine/Vannucci model [7]. Animals, recovered for 2 h after surgery, were then exposed to hypobaric hypoxia as previously described. Sham control animals were submitted to surgery without vessel sectioning and then kept in the chamber under normobaric normoxic conditions. In all cases, the survival rate was 100% and animals were anesthetized with ketamine (100 mg/Kg body weight, i.p.) and xylazine (5 mg/Kg body weight, i.p.) and killed after the hypobaric chamber was opened. Body temperature was monitored and maintained throughout all procedures.

The left-brain cortices from animals of all experimental groups were extracted and processed according to the following procedure: 0.1 g of the cortices were homogenized with 1.5 mL of extraction buffer pH 8.0 containing 8 M urea, 20 mM dithiothreitol (DTT), 100 mM Tris–HCl, 0.75 mM phenylmethylsulfonyl fluoride (PMSF), and 4% 3-[(3-cholamidopropyl)-dimethylammonio]-1-propane sulfonate (CHAPS). Proteins were extracted in this buffer for 60 min on ice. Every 15 min, the samples were moderately shaken in a vortex and afterwards were centrifuged at 10 000 × *g* for 15 min at 4°C. The protein concentration of supernatants was measured using the CB-XTM Protein Assay (G-Biosciences, St Louis, USA). Lessening of detergents from protein extraction buffer was carried out using 100 mM triethylammonium bicarbonate (TEAB) by ultrafiltration (millipore 3 k) during 30 min at 12 500 rpm and precipitation (BioRad Protein Sample Cleanup). Isobaric Label Reagent Set (Thermo TMTsixplex™) was performed following the manufacturer's instructions, and followed by desalting (100 mg C18 cartridges, Schalau). Experiments and analysis were performed in blind manner.

The different experimental conditions were then distributed into four different Tandem mass Tag™ (TMTsixplex™) labeled samples, which were analysed using a LTQ Orbitrap mass spectrometer (Thermo Fisher Scientific). Briefly, peptides were analyzed with the Orbitrap mass spectrometer equipped with a nano UHPLC Ultimate 3000 (Dionex-Thermo Scientifics). Chromatography conditions were: mobile phase solution A: 0.1% formic acid in ultrapure water; mobile phase solution B: 80% acetonitrile, 0.1% formic acid, in a C18 nanocapillary column (Acclaim PepMap C18, 75 um internal diameter, 1.8 um particle size, Dionex-Thermo Scientifics) as follow: 5 min, 4% solution B; 240 min, 4–35% solution B; 10 min, 35–80% B; 10 min, 80% B; 10 min 4% B. Nanoelectrospray voltage was set to 1300 V and capillary voltage to 50 V at 190C°. The LTQ Orbitrap was operated in parallel mode, allowing for the accurate measurement of the precursor survey scan (400–1500 *m/z*) in the Orbitrap selection, a 30 000 full-width at half-maximum (FWHM) resolution at *m/z* 400 concurrent with the acquisition of three CID/HCD Data-Dependent MS/MS scans in the LIT and C-Trap for peptide sequence and isotopes quantitation (100–2000 *m/z*), respectively. HCD Resolution set to 7500 FWHM at *m/z* 400. Singly charged ions were excluded. The normalized collision energies were 40% for HCD and 35% for CID. The maximum injection times for MS and MS/MS were set to 50 and 500 ms, respectively. The precursor isolation width was 3 amu and the exclusion mass width was set to 5 ppm. Monoisotopic precursor selection was allowed and singly charged species were excluded. A more extensive description of the experimental procedures and a MIAPE [8] compliant report are found in Supporting Information Methods.

The MS proteomics data have been deposited to the ProteomeXchange Consortium via the PRIDE [9] partner repository with the dataset identifier PXD004091 (Username: reviewer12476@ebi.ac.uk, Password: tAAJD9QV). Data were analyzed afterwards using Proteome Discoverer (Thermo Fisher Scientific) and searched against a Uniprot Proteome of *Rattus norvegicus* database, containing 27 820 sequences (version 2015.01), resulting in the initial identification of 1409 proteins. Of this initial set of proteins, only 339 were further used in this study as confidently quantified. For a protein to be considered so, it had to present at least two identified peptides with FDR<5%, present quantitative information into the three groups of the analysis (HH, HHI, and control) and its quantitation tags with a coefficient of variation inferior to 30%. The complete list of 339 quantified proteins can be consulted in Supporting Information Data. Of these proteins, only 99 showed differential expression with respect to the control in HH, HHI, or both conditions (Table 1). The variability of a given protein is reported as the amount of positive or negative variation evidence: taking the global standard deviation of the ratios distribution (g.s.d.) as threshold, proteins over/under expressed more than two units of g.s.d. in the same technical replicate, or between 1.5 and two

Table 1. List of 99 rat proteins expressed differentially in HH and HHI with Uniprot accession, gene symbol, description, ratios, and overall evidence of variation: "++" high, "+" moderate, "−−" high, and "−" moderate evidence of over and underexpression, respectively, and " = " for unchanged expression

Protein	Gene	Description	HH data	ΔHH	HHI data	ΔHHI
G3V6Y6	Pygb	α-1,4 glucan phosphorylase	0.63 ± 0.2 0.80 ± 0.2	−	0.70 ± 0.1	−
G3V9G3	Camk2b	Ca/calmodulin-dep. PK II, β, isof.CRA_a	1.02 ± 0.3 0.62 ± 0.2	−	0.69 ± 0.1 0.88 ± 0.1	−
P11275	Camk2a	Ca/calmodulin-dep.PK type II sub.α	0.99 ± 0.2 0.63 ± 0.1	−	0.93 ± 0.1 0.72 ± 0.1	−
P50554	Abat	4-aminobutyrate aminotransf. Mitoch	0.95 ± 0.1 0.63 ± 0.0	−	0.73 ± 0.1	−
F1LRK1	Atp4a	K-transporting ATPase α chain 1	0.57 ± 0.1 0.88 ± 0.1	−	0.59 ± 0.1	−−
F1M779	Cltc	Clathrin heavy chain	0.78 ± 0.2 0.63 ± 0.1	−	0.64 ± 0.1 0.82 ± 0.1	−−
G3V846	Slc1a3	Amino acid transporter	0.62 ± 0.0 0.64 ± 0.1	−	0.93 ± 0.2 0.62 ± 0.0	−−
P06685	Atp1a1	Na/K-transporting ATPase sub. α-1	0.63 ± 0.2	−	0.64 ± 0.1 0.96 ± 0.1	−−
P06686	Atp1a2	Na/K-transporting ATPase sub. α-2	0.62 ± 0.1	−	0.63 ± 0.1 0.96 ± 0.1	−−
P06687	Atp1a3	Na/K-transporting ATPase sub. α-3	0.61 ± 0.1	−	0.94 ± 0.1 0.63 ± 0.1	−−
P32851	Stx1a	Syntaxin-1A	0.96 ± 0.0 0.63 ± 0.1	−	0.95 ± 0.2 0.64 ± 0.1	−−
Q06645	Atp5g1	ATP synthase F(0) complex sub.C1,mitoch	0.53 ± 0.0 0.82 ± 0.0	−	0.60 ± 0.0 0.92 ± 0.1	−−
Q6AXX6	Fam213a	Redox-regulatory protein FAM213A	0.68 ± 0.1 0.64 ± 0.0	−	0.63 ± 0.0	−−
Q6PDU7	Atp5l	ATP synthase sub. g, mitochondrial	0.85 ± 0.1 0.60 ± 0.1	−	1.42 ± 0.1 0.77 ± 0.1	++
D3ZAF6	Atp5j2	ATP synthase sub. f, mitochondrial	0.62 ± 0.1 0.72 ± 0.0	−	0.99 ± 0.0 0.75 ± 0.1	=
F7EYB9	Omg	Protein Omg	0.90 ± 0.0 0.68 ± 0.1	−	0.85 ± 0.1 0.92 ± 0.0	=
P07825	Syp	Synaptophysin	0.61 ± 0.0	−	0.93 ± 0.1 0.74 ± 0.1	=
Q4KLX9	Ccdc163	Protein Ccdc163	0.62 ± 0.1 0.89 ± 0.0	−	0.98 ± 0.0	=
Q63564	Sv2b	Synaptic vesicle glycoprotein 2B	0.60 ± 0.1 0.73 ± 0.2	−	0.81 ± 0.1	=
Q5RKJ9	Rab10	RAB10, member RAS oncogene family	0.54 ± 0.0 0.54 ± 0.0	−−	0.62 ± 0.0 0.95 ± 0.2	−−
P84087	Cplx2	Complexin-2	1.33 ± 0.4 0.50 ± 0.1	−−	1.15 ± 0.3 1.35 ± 0.3	+
B0BNE6	Ndufs8	NADH-DH(Ubiq.)Fe-S prot8 (Pred),isoCRA_a	0.45 ± 0.1 1.22 ± 0.1	−−	1.17 ± 0.2 1.07 ± 0.1	=
P84817	Fis1	Mitochondrial fission 1 protein	0.90 ± 0.2 0.57 ± 0.0	−−	0.92 ± 0.1	=
D3ZH42	Mov10l1	Protein Mov10l1	1.34 ± 0.1 1.05 ± 0.0	+	0.65 ± 0.0	−
P02770	Alb	Serum albumin	0.75 ± 0.1 1.31 ± 0.3	+	0.68 ± 0.1 0.99 ± 0.1	−
D3ZF13	LOC683884	Acyl carrier protein	0.81 ± 0.0 1.40 ± 0.1	+	1.31 ± 0.1	+
P04692	Tpm1	Tropomyosin α-1 chain	1.37 ± 0.2	+	1.28 ± 0.2	+
P26772	Hspe1	10 kDa heat shock protein, mitochondrial	1.46 ± 0.4 1.05 ± 0.3	+	0.95 ± 0.1 1.27 ± 0.3	+
P31399	Atp5h	ATP synthase sub. d, mitochondrial	1.45 ± 0.3	+	1.27 ± 0.3	+

(*Continued*)

Table 1. Continued

Protein	Gene	Description	HH data	ΔHH	HHI data	ΔHHI
P80254	Ddt	D-dopachrome decarboxylase	1.39 ± 0.2	+	1.27 ± 0.1	+
Q03344	Atpif1	ATPase inhibitor, mitochondrial	1.44 ± 0.2	+	1.31 ± 0.2	+
			1.14 ± 0.1		1.08 ± 0.1	
Q6TXF3	Dbi	Acyl-CoA-binding protein	0.97 ± 0.1	+	1.28 ± 0.2	+
			1.41 ± 0.1			
P07171	Calb1	Calbindin	1.39 ± 0.1	+	1.37 ± 0.2	++
			0.85 ± 0.1			
P08082	Cltb	Clathrin light chain B	1.21 ± 0.3	+	1.31 ± 0.1	++
			1.42 ± 0.2		1.27 ± 0.0	
B2RYS2	Uqcrb	Cytochrome b-c1 complex sub. 7	1.44 ± 0.1	+	1.13 ± 0.1	=
			0.85 ± 0.2		1.08 ± 0.2	
D3ZD09	Cox6b1	Cytochrome c oxidase sub. 6B1	1.41 ± 0.3	+	1.23 ± 0.2	=
					1.14 ± 0.2	
D3ZJ08	Hist2h3c2	Histone H3	1.00 ± 0.1	+	1.17 ± 0.0	=
			1.31 ± 0.2		1.22 ± 0.2	
D4A0T0	Ndufb10	Protein Ndufb10	1.45 ± 0.0	+	1.11±0.1	=
D4A678	Spta1	Protein Spta1	0.85 ± 0.1	+	1.01±0.0	=
			1.39 ± 0.1			
D4ACQ2	LOC690384	Protein LOC690384	1.37 ± 0.0	+	1.22±0.1	=
			1.07 ± 0.1			
F1LMR7	Dpp6	Dipeptidyl aminopeptidase-like p6	1.33 ± 0.2	+	0.80±0.0	=
F1M269	NA	Glyceraldehyde-3-phosphate DH Frag.	1.08 ± 0.1	+	1.09±0.1	=
			1.40 ± 0.2			
G3V6D3	Atp5b	ATP synthase sub. β	1.40 ± 0.4	+	1.14 ± 0.2	=
			0.81 ± 0.2		1.12 ± 0.2	
G3V6 × 7	Pcsk1n	Proprot. convertase subtilisin/kexin T1 inhib	1.39 ± 0.4	+	1.11 ± 0.1	=
					1.25 ± 0.3	
G3V8Q2	Ina	α-internexin	1.37 ± 0.3	+	0.96 ± 0.1	=
					1.06 ± 0.2	
O88339	Epn1	Epsin-1	1.44 ± 0.1	+	1.12±0.1	=
P05065	Aldoa	Fructose-bisphosphate aldolase A	0.94 ± 0.1	+	0.89 ± 0.1	=
			1.33 ± 0.4		1.03 ± 0.1	
P10860	Glud1	Glutamate DH 1, mitochondrial	0.93 ± 0.1	+	1.04 ± 0.1	=
			1.39 ± 0.4		0.99 ± 0.1	
P17764	Acat1	Acetyl-CoA acetyltrans. Mitoch.	1.09 ± 0.0	+	1.12±0.0	=
			1.32 ± 0.1			
P23565	Ina	α-internexin	1.37 ± 0.4	+	0.96 ± 0.1	=
					1.06 ± 0.2	
P34926	Map1a	Microtubule-associated protein 1A	1.09 ± 0.2	+	1.08 ± 0.2	=
			1.31 ± 0.3		1.00 ± 0.2	
P35332	Hpcal4	Hippocalcin-like prot. 4	1.40 ± 0.3	+	1.13±0.2	=
			0.95 ± 0.2			
P47819	Gfap	Glial fibrillary acidic protein	1.11 ± 0.2	+	1.15 ± 0.2	=
			1.42 ± 0.4		1.04 ± 0.2	
P48500	Tpi1	Triosephosphate isomerase	1.07 ± 0.1	+	1.06 ± 0.1	=
			1.38 ± 0.3		1.00 ± 0.1	
P54311	Gnb1	Guanine nucl-bind prot G(I)/G(S)/G(T) sub. β-1	0.82 ± 0.1	+	1.04 ± 0.1	=
			1.32 ± 0.1		0.91 ± 0.2	
P54313	Gnb2	Guanine nucl-bind prot G(I)/G(S)/G(T) sub. β-2	0.78 ± 0.1	+	0.91±0.0	=
			1.32 ± 0.1			
P62161	Calm1	Calmodulin	1.44 ± 0.4	+	1.19±0.2	=
P62762	Vsnl1	Visinin-like protein 1	1.39 ± 0.3	+	1.00 ± 0.2	=
			0.88 ± 0.2		1.20 ± 0.1	
P63329	Ppp3ca	Ser/Thr-prot Pase 2B catalytic sub. α isof	0.70 ± 0.1	+	0.81 ± 0.2	=
			1.35 ± 0.3		0.96 ± 0.1	
P85845	Fscn1	Fascin	1.33 ± 0.4	+	1.10 ± 0.2	=
			0.87 ± 0.1		0.99 ± 0.3	

(*Continued*)

Table 1. Continued

Protein	Gene	Description	HH data	ΔHH	HHI data	ΔHHI
Q5XIF3	Ndufs4	NADH DH [ubiquinone] Fe-S prot4, mitoch	1.25 ± 0.2 1.34 ± 0.4	+	0.99±0.3	=
Q8R2H0	Atp6v1g2	ATPase, H+ transporting, V1 sub. G isoform 2	1.32 ± 0.4 1.33 ± 0.2	+	1.19±0.1	=
F1LQ96	Sncg	Gamma-synuclein	1.44 ± 0.1 1.60 ± 0.1	++	1.27±0.1	+
G3V7Y3	Atp5d	ATP synthase sub. delta, mitochondrial	1.63 ± 0.2 1.11 ± 0.1	++	0.97 ± 0.1 1.32 ± 0.1	+
P07936	Gap43	Neuromodulin	1.62 ± 0.3	++	1.28±0.4	+
D3ZH98	NA	Uncharacterized protein	1.55 ± 0.2 1.59 ± 0.5	++	1.38±0.2	++
F1LMW7	Marcks	Myristoylated Ala-rich C-kinase substrate	1.52 ± 0.1 0.88 ± 0.2	++	1.38 ± 0.1	++
Q05175	Basp1	Brain acid soluble protein 1	1.78 ± 0.3	++	1.55 ± 0.2 1.07 ± 0.0	++
D3ZCZ9	LOC100912599	Protein LOC100912599	1.52 ± 0.2	++	0.92 ± 0.0	=
D4AB12	NA	Uncharacterized protein	1.46 ± 0.2 1.08 ± 0.1	++	1.13 ± 0.1	=
P56571	NA	ES1 protein homolog, mitochondrial	1.58 ± 0.4 0.99 ± 0.2	++	1.04 ± 0.0	=
Q3ZB98	Bcas1	Breast carcinoma-ampl.seq1.hom(Frag)	1.71 ± 0.2 1.54 ± 0.4	++	1.10 ± 0.2	=
Q63754	Sncb	β-synuclein	1.54 ± 0.2 1.45 ± 0.3	++	1.21 ± 0.1	=
P01946	Hba1	Hemoglobin sub. α-1/2	0.96 ± 0.1 0.97 ± 0.2	=	0.65 ± 0.2	-
P02688	Mbp	Myelin basic protein	1.09 ± 0.1	=	0.74 ± 0.1 0.81 ± 0.1	-
P04631	S100b	Protein S100-B	1.31 ± 0.4 0.89 ± 0.2	=	1.12 ± 0.1 0.80 ± 0.0	-
P05708	Hk1	Hexokinase-1	0.80 ± 0.1 0.68 ± 0.1	=	0.93 ± 0.1 0.69 ± 0.1	-
P21707	Syt1	Synaptotagmin-1	0.95 ± 0.2 0.70 ± 0.1	=	0.91 ± 0.1 0.70 ± 0.1	-
P27139	Ca2	Carbonic anhydrase 2	0.79 ± 0.1 0.75 ± 0.1	=	0.72 ± 0.1	-
P31596	Slc1a2	Excitatory amino acid transporter 2	0.80 ± 0.2 0.68 ± 0.1	=	1.04 ± 0.3 0.71 ± 0.2	-
P62944	Ap2b1	AP-2 complex sub. β	0.64 ± 0.2 0.94 ± 0.0	=	1.02 ± 0.1 0.68 ± 0.0	-
Q09073	Slc25a5	ADP/ATP translocase 2	0.90 ± 0.2 0.65 ± 0.1	=	0.68 ± 0.1 0.95 ± 0.1	-
Q6P6V0	Gpi	Glucose-6-phosphate isomerase	0.93 ± 0.2 0.70 ± 0.1	=	0.73 ± 0.1 1.02 ± 0.0	-
Q812E9	Gpm6a	Neuronal membrane glycoprotein M6-a	0.73 ± 0.1	=	0.71 ± 0.2 0.91 ± 0.0	-
B0K020	Cisd1	CDGSH Fe-S domain-cont. Prot1	1.02 ± 0.1 0.81 ± 0.2	=	0.84 ± 0.1 0.60 ± 0.1	- -
D3ZNI9	Kcnt1	K channel subfamily T member 1	0.98 ± 0.3 0.91 ± 0.1	=	0.61 ± 0.1	- -
G3V9B3	Mag	Myelin-associated glycoprotein	0.67 ± 0.0	=	0.59 ± 0.0 0.84 ± 0.1	- -
P02091	Hbb	Hemoglobin sub. β-1	0.93 ± 0.1	=	0.61 ± 0.1	- -
P13233	Cnp	2′,3′-cyclic-nucleotide 3′-Pdiesterase	1.19 ± 0.3 0.68 ± 0.1	=	0.60 ± 0.1 0.83 ± 0.2	- -
Q05962	Slc25a4	ADP/ATP translocase 1	0.78 ± 0.2 0.64 ± 0.2	=	0.63 ± 0.1 0.94 ± 0.1	- -
Q62669	NA	Protein Hbb-b1	1.09 ± 0.2 0.97 ± 0.2	=	0.64 ± 0.1	- -

(*Continued*)

Table 1. Continued

Protein	Gene	Description	HH data	ΔHH	HHI data	ΔHHI
Q63345	Mog	Myelin-oligodendrocyte glycoprotein	0.64 ± 0.1	=	0.58 ± 0.1 0.85 ± 0.1	- -
Q8SEZ5	NA	Cytochrome c oxidase sub. 2	0.71 ± 0.0	=	0.61 ± 0.1	- -
R9PY00	Vamp2	Vesicle-assoc membr. prot2 (Frag)	0.94 ± 0.2	=	0.76 ± 0.0	- -
B2GV73	Arpc3	Actin-related protein 2/3 complex sub. 3	0.94 ± 0.0 0.95 ± 0.1	=	0.98 ± 0.0 1.22 ± 0.2	+
P25113	Pgam1	Phosphoglycerate mutase 1	1.01 ± 0.2 1.35 ± 0.2	=	1.30 ± 0.4	+
P47728	Calb2	Calretinin	1.29 ± 0.2 0.93 ± 0.1	=	1.30 ± 0.2 1.01 ± 0.2	+
F1M2D3	Vdac1	Uncharacterized protein	1.23 ± 0.2 1.13 ± 0.3	=	1.28 ± 0.2 1.16 ± 0.2	+ +
Q9Z2L0	Vdac1	Voltage-dep anion-sel. channel prot1	1.19 ± 0.2 1.07 ± 0.3	=	1.28 ± 0.2 1.12 ± 0.2	+ +

g.s.d. in two technical replicates, are considered as highly over/under expressed, while variation between 1.5 and two g.s.d in a single technical replicate is considered as moderate evidence of over/under expression (Supporting Information Analysis).

Using Cytoscape ClueGO plug-in [10], we performed a Gene Ontology (GO) enrichment analysis (two-sided hypergeometric test and Bonferroni step-down correction) of the 99 proteins expressed differentially in HH and/or HHI conditions: 54 of them belong to at least one of the 20 enriched biological processes found. Both hypoxic models present a similar number of differentially expressed proteins (37 and 36, respectively), but with an overall positive expression in HH (22 overexpressed proteins) and negative in HHI (25 underexpressed proteins) (Fig. 1). The similar set of affected processes, both in HH and HHI, points to similar pathologic patterns [1], while the overall inhibitory nature found in HHI is explained by its greater severity in contrast to HH [5].

The 20 biological processes identified were grouped into seven functional groups attending to the similarity of the processes and genes shared (Fig. 2):

(i) ATP metabolic process and (ii) Proton, Hydrogen transmembrane, and Inorganic cation transport, both showing higher enrichment in HH, present a more downregulated state in HHI: potassium import across plasma membrane is severely inhibited (Atp1a1, Atp1a3), while calcium

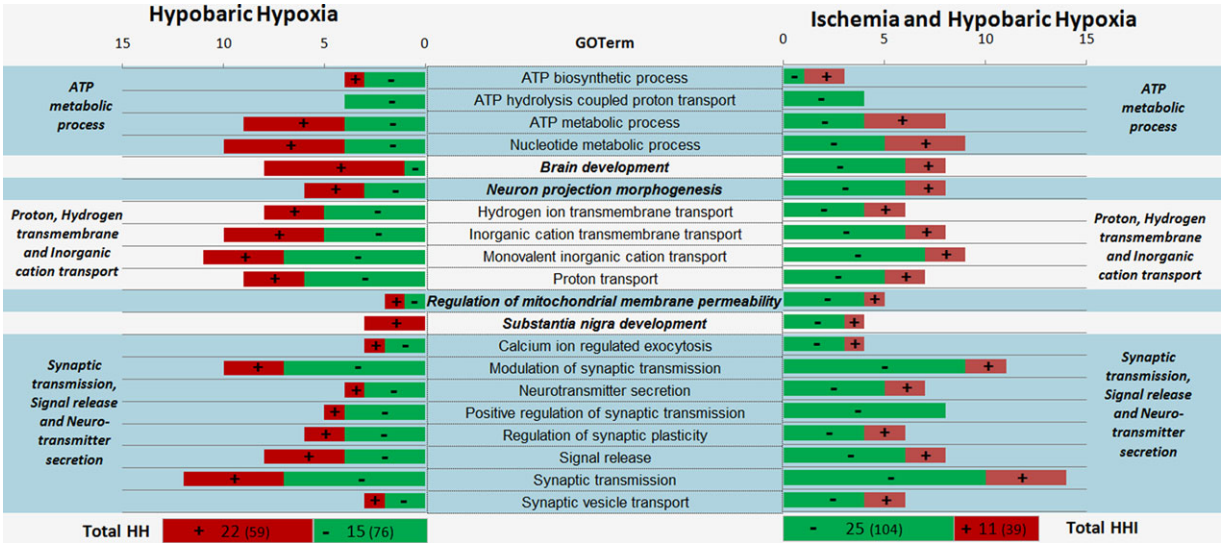

Figure 1. The proportion of over/underexpressed proteins in HH (37 proteins) and HHI (36 proteins) is shown for each of the 20 GO biological processes, grouped into seven functional groups (bold). Under the bar chart, the total of over/underexpressed proteins (in parentheses the number of times these proteins appear into one biological process), shows a general increase of protein expression in HH (22 protein with increased levels versus 15 decreased) and decrease in HHI (25 decreased versus 11 increased).

A

GO ID	Functional group	HH Pval	HHI Pval	Condition
GO:0046902	Regulation of mitochondrial membrane permeability	4.2E-01	**4.3E-05**	HHI
GO:0021762	Substantia nigra development	2.1E-02	**8.3E-04**	HHI
GO:0017156	Synaptic transmission, Signal release and Neuro-transmitter secretion	3.3E-01	**4.5E-02**	HHI
GO:0050804		1.6E-04	**2.0E-05**	
GO:0007269		1.0E-01	**1.1E-04**	
GO:0050806		1.9E-02	**1.4E-05**	
GO:0048167		4.1E-03	4.1E-03	
GO:0023061		2.5E-02	2.5E-02	
GO:0007268		5.1E-04	**1.5E-05**	
GO:0048489		4.0E-01	**5.0E-04**	

GO ID	Functional group	HH Pval	HHI Pval	Condition
GO:0048812	Neuron projection morphogenesis	6.8E-01	**6.3E-02**	HHI
GO:0006754	ATP metabolic process	**1.1E-03**	2.2E-02	HH
GO:0015991		4.6E-04	4.6E-04	
GO:0046034		**1.3E-05**	1.4E-04	
GO:0009117		**9.7E-03**	4.0E-02	
GO:1902600	Proton, Hydrogen transmembrane and Inorganic cation transport	**1.4E-07**	4.5E-05	HH
GO:0098662		**3.9E-03**	6.5E-02	
GO:0015672		**3.6E-04**	8.9E-03	
GO:0015992		**7.8E-08**	1.9E-05	
GO:0007420	Brain development	4.4E-01	4.4E-01	HH/HHI

B

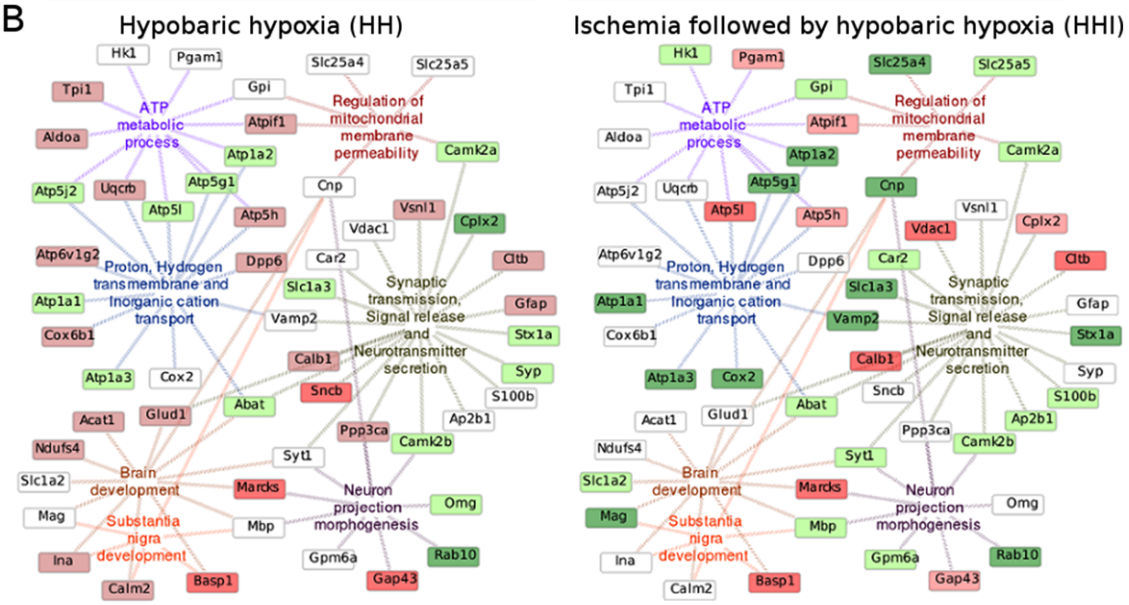

C

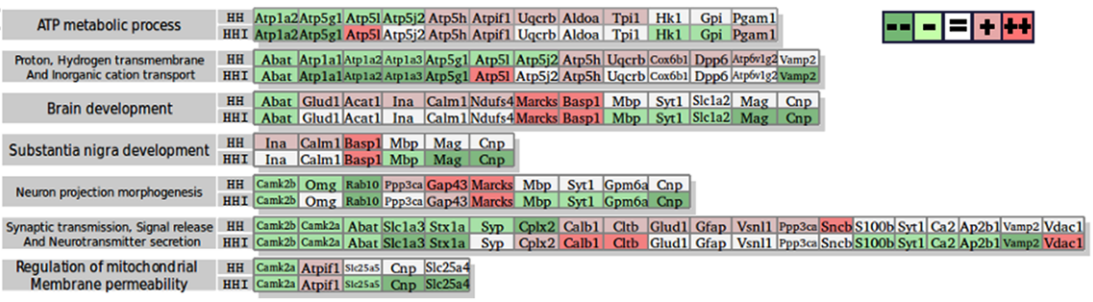

Figure 2. Gene enrichment analysis in HH and HHI. (A) Table showing GO terms associated to each functional group, *p*-values obtained for HH and HHI related genes (in bold the lowest) and condition (HH or HHI) in which the functional group is more enriched. (B) Relationships between functional groups and genes in HH and HHI. Genes are coloured dark and light green for high and moderate evidence of under expression, and dark and light red for high and moderate evidence of overexpression, respectively. (C) For each functional group, using the same legend, the list of genes related to HH and HHI experimental conditions.

exocytosis is also downregulated (Atp1a2 and Vamp2). Furthermore, response to hypoxia (Aldoa) and response to ischemia (HK1) markers [11] show differential expression on their respective conditions.

(iii) Brain development, (iv) Neuron projection morphogenesis, and (v) *Substantia nigra* development present upregulated genes—Gap43, Maks, and Basp1—all highly involved in signal transduction pathways, membrane transport and cytoskeletal dynamics [12]. The calmodulin-dependent protein kinases (Camk2a and Camk2b), that phosphorylate the central bioenergy sensor AMP-activated protein kinase [13], are downregulated in both HH and HHI; this same tendency is followed by Rab10, a small GTPase acting as regulator of membrane trafficking and fusion also involved in autophagy [14]. Additionally, several proteins related to substantia nigra development (Ina, Calm1, Mbp, Mag, and Cnp) show variation in HH and HHI, consistently with previous proteomic studies of changes in *Substantia nigra* caused by neurodegenerative diseases [15].

(vi) Synaptic transmission, Signal release, and Neurotransmitter secretion are greatly impaired under HHI, as expected under severe excitotoxic damage; interestingly,

the SNARE protein Vamp2, and its regulatory proteins Syt1, both highly involved in glutamate release and neuron damage after ischemic injury, are downregulated but only in HHI [16].

(vii) Regulation of mitochondrial membrane permeability points to the activation of apoptosis through mitochondrial pathways (downregulation of apoptosis inhibitors Gpi, Slc25a4 Slc25a5, and activation of Atpif1). Components of the mPTP (adenine nucleotide translocator: Slc25a4, Slc25a5, and Vdac1) [17] where also differentially expressed in HH and HHI.

In conclusion, HHI model presents a global effect of protein downregulation while HH produces an overall increase of the protein levels. With HH mainly affecting oxidative and energetic metabolism, HHI also interferes with synaptic transmission, neurotransmitter secretion, *substantia nigra* development and triggers apoptosis through mitochondrial pathway.

This study was supported by the Spanish Ministry of Science and Innovation (SAF2008-03938).

The authors have declared no conflict of interest.

2 References

[1] Dugan, L. L., Choi, D. W., Hypoxia-ischemia and brain infarction. In *Basic Neurochemistry: Molecular, Cellular and Medical Aspects*. 6th edition (Eds.: Siegel, G. J., Agranoff, B. W., Albers, R. W., Fisher, S. K., Uhler, M. D.). Lippincott Williams and Wilkins, Philadelphia 1999.

[2] Granger, D. N., Kvietys, P. R., Reperfusion injury and reactive oxygen species: the evolution of a concept. *Redox Biol.* 2015, *6*, 524–551.

[3] Aarts, M. M., Arundine, M., Tymianski, M., Novel concepts in excitotoxic neurodegeneration after stroke. *Expert Rev. Mol. Med.* 2003, *5*, 1–22.

[4] Peinado, M. A., del Moral, M. L., Esteban, F. J., Martínez-Lara, E. et al., Aging and neurodegeneration: molecular and cellular bases. *Rev. Neurol.* 2000, *31*, 1054–1065.

[5] Rocha-Ferreira, E., Hristova, M., Plasticity in the neonatal brain following hypoxic-ischaemic injury. *Neural Plast.* 2016, *2016*, 4901014.

[6] Hernández, R., Blanco, S., Peragón, J., Pedrosa, J. Á., Peinado, M. Á. et al., Hypobaric hypoxia and reoxygenation induce proteomic profile changes in the rat brain cortex. *Neuromol. Med.* 2013, *15*, 82–94.

[7] Adhami, F., Liao, G., Morzov, Y. M. ,Schloemer, A. et al., Cerebral ischemia-hypoxia induces intravascular coagulation and autophagy. *Am. J. Pathol.* 2006, *169*, 566–583.

[8] Taylor, C. F., Paton, N. W., Lilley, K. S., Binz, P. A. et al., The minimum information about a proteomics experiment (MIAPE). *Nat. Biotechnol.* 2007, *25*, 887–893.

[9] Vizcaíno, J. A., Côté, R. G., Csordas, A., Dianes, J. A. et al., The PRoteomics IDEntifications (PRIDE) database and associated tools: status in 2013. *Nucleic Acids Res.* 2013, *41*(Database issue), D1063–D1069.

[10] Bindea, G., Mlecnik, B., Hackl, H., Charoentong, P. et al., ClueGO: a Cytoscape plug-in to decipher functionally grouped gene ontology and pathway annotation networks. *Bioinforma. Oxf. Engl.* 2009, *25*, 1091–1093.

[11] Pasdois, P., Parker, J. E., Griffiths, E. J., Halestrap, A. P. et al., The role of oxidized cytochrome c in regulating mitochondrial reactive oxygen species production and its perturbation in ischaemia. *Biochem J.* 2011, *436*, 493–505.

[12] Sandal, M., Paltrinieri, D., Carloni, P., Musiani, F., Giorgetti, A. et al., Structure/function relationships of phospholipases C Beta. *Curr. Protein Pept. Sci.* 2013, *14*, 650–657.

[13] Khatri, N., Man, H.-Y., Synaptic activity and bioenergy homeostasis: implications in brain trauma and neurodegenerative diseases. *Front Neurol.* 2013, *4*, 199.

[14] Szatmári, Z., Sass, M., The autophagic roles of Rab small GTPases and their upstream regulators. *Autophagy* 2014, *10*, 1154–1166.

[15] Chen, S., Lu, F. F., Seeman, P., Liu, F. et al., Quantitative proteomic analysis of human substantia nigra in Alzheimer's disease, Huntington's disease and multiple sclerosis. *Neurochem. Res.* 2012, *37*, 2805–2813.

[16] Wang, Z., Wei, X., Liu, K., Yang, F. et al., NOX2 deficiency ameliorates cerebral injury through reduction of complexin II-mediated glutamate excitotoxicity in experimental stroke. *Free Radic. Biol. Med.* 2013, *65*, 942–951.

[17] Tanno, M., Miura, T., Adenine nucleotide translocator, a mitochondrial carrier protein, and fate of cardiomyocytes after ischaemia/reperfusion. *Cardiovasc. Res.* 2008, *80*, 1–2.

